

## An efficient seismic analysis of regular skeletal structures via graph product rules and canonical forms

A. Kaveh\* and P. Zakian<sup>a</sup>

Centre of Excellence for Fundamental Studies in Structural Engineering, School of Civil Engineering, Iran University of Science and Technology, Narmak, Tehran-16, Iran

(Received June 2, 2015, Revised September 1, 2015, Accepted October 28, 2015)

**Abstract.** In this study, graph product rules are applied to the dynamic analysis of regular skeletal structures. Graph product rules have recently been utilized in structural mechanics as a powerful tool for eigensolution of symmetric and regular skeletal structures. A structure is called regular if its model is a graph product. In the first part of this paper, the formulation of time history dynamic analysis of regular structures under seismic excitation is derived using graph product rules. This formulation can generally be utilized for efficient linear elastic dynamic analysis using vibration modes. The second part comprises of random vibration analysis of regular skeletal structures via canonical forms and closed-form eigensolution of matrices containing special patterns for symmetric structures. In this part, the formulations are developed for dynamic analysis of structures subjected to random seismic excitation in frequency domain. In all the proposed methods, eigensolution of the problems is achieved with less computational effort due to incorporating graph product rules and canonical forms for symmetric and cyclically symmetric structures.

**Keywords:** seismic analysis; regular skeletal structures; graph product rules; canonical forms

---

### 1. Introduction

In spite of advances in computational technology for executing large-scale engineering problems, efficient and swift analysis of structures is still necessary in order to reduce the required memory and computational time. An analysis is known as optimal analysis when it uses sparse, well-structured and well-conditioned structural matrices. This type of analysis is particularly effective for analysis of large-scale structures. Recent advances and developments of graph theoretical matrix methods for optimal structural analysis in computational structural mechanics are thoroughly discussed in Kaveh (2013).

Form-finding in symmetric structures is very popular among researchers, Kangwai *et al.* (1999). Here, we mention only a few of such studies which are more relevant to this work. Williams (1986) presented efficient eigenvalue analysis of rotationally symmetric structures. Dynamic analysis of cyclic symmetric structures was performed by McDaniel and Chang (1980), Olson *et al.* (2014), and Shi *et al.* (2014, 2015). Thomas (1979) utilized Fourier transform and

---

\*Corresponding author, Professor, E-mail: [alikaveh@iust.ac.ir](mailto:alikaveh@iust.ac.ir)

<sup>a</sup>MSc Student

modal information for this kind of analysis. He *et al.* (2013) developed a scaled boundary finite element method for elastic analysis of cyclically symmetric two dimensional problems. On the other hand, Kaveh (2013) used graph product rules as an efficient tool for configuration processing and eigensolution of cyclic symmetric structures. Kaveh and Rahami (2010) developed graph product rules for static analysis of repetitive structures. Force method based efficient analysis of cyclic symmetric structures was fulfilled by Koohestani (2011). Kaveh and Nemati (2010) employed canonical forms for eigensolution and stability analysis of rotationally repetitive structures considering geometric stiffness matrix. Closed-form eigensolutions of matrices having special patterns is due to Yueh (2005). This is expanded to canonical forms and eigensolution of symmetric structures by Kaveh (2013). Further applications of product graphs and regular structures are due to El-Raheb (2011) who worked on modal analysis of cyclic symmetric hexagon lattice, Koohestani and Kaveh (2010) expanded the concept of canonical forms to efficient buckling and free vibration analysis of cyclically repeated space truss structures, Rahami *et al.* (2015) performed swift structural analysis followed by optimal design using efficient matrix methods, and Zingoni used group theoretical approaches for efficient dynamic analysis of symmetric structures (2012, 2014).

This study uses graph product rules and canonical forms for dynamic analysis of symmetric structures subjected to earthquake loading. Symmetry is a general concept and dynamic analysis of cyclic symmetric structures, are investigated in the first part of this paper. In the second part, random dynamic analysis in frequency domain is performed for repetitive structures under seismic excitation, incorporating canonical forms and closed-form eigensolution. Graph products constitute an important field of graph theory that focuses on regular and repetitive patterns and their properties. A structure is called *regular* if the underlying model is a product graph. The subgraphs producing a product graph are known as its *generators*. Initially, formulation of time history dynamic analysis of these structures under seismic excitation employing graph product rules is proposed. These formulations can generally be employed for linear elastic dynamic analysis using modal data. Random vibration analysis of regular repetitive structures is then presented utilizing canonical forms and closed-form eigensolution of matrices containing prevalent pattern for symmetric structures. In this section, the structures are subjected to random seismic excitation. In the proposed methods, the main improvement is due to the eigensolution of problems with much less computational effort.

## 2. Graph product rules for static analysis

Graph product rules for static analysis of repetitive structures have been proposed by Kaveh and Rahami (2010), and briefly reviewed herein. The necessary and sufficient condition for simultaneous diagonalization of the Hermitian matrices  $\mathbf{A}_i$  and  $\mathbf{A}_j$  using orthogonal matrix is their commutative property, that is

$$\mathbf{A}_i \mathbf{A}_j = \mathbf{A}_j \mathbf{A}_i \quad (i \neq j) \quad (1)$$

Suppose a matrix  $\Lambda$  can be written as the sum of  $n$  Kronecker products as

$$\Lambda = \sum_{i=1}^n \mathbf{A}_i \otimes \mathbf{B}_i \quad (2)$$



$$\Delta = \sum_{i=1}^{mm} \frac{\{\Phi_i\} \langle \Phi_i \rangle}{\lambda_i} \mathbf{P} \quad (7)$$

$\{\cdot\}$  and  $\langle \cdot \rangle$  denote column and row matrices (vectors), respectively. Since  $\mathbf{K}$  is expressed in cylindrical coordinate system, the load vector  $\mathbf{P}$  should also be considered in this coordinate system. Significant advantage of this method is its rapid eigenvalue analysis, and there is no need to inverse the matrix  $\mathbf{K}$ . However, it is worth mentioning that the eigenvectors should be normalized here. This normalization is automatically performed by normalizing each component of the Kronecker products in Eq. (5). The calculated  $\Delta$  must be converted to Cartesian coordinate system as discussed later.

### 3. Graph product rules for dynamic analysis

In this part, graph product based methods are developed for dynamic analysis of cyclically symmetric structures. Here, formulations are presented for time history analysis. Nevertheless, these can readily be simplified to spectral dynamic analysis. Here, time history analysis is performed using modal analysis. In order to conduct time integration, Newmark-Beta method with average acceleration is implemented for its unconditional stability property and accuracy.

#### 3.1 Element matrices for dynamic analysis of truss structures

For 3D truss analysis, stiffness and lumped mass matrices of an element are defined as

$$\begin{aligned} \hat{\mathbf{k}}_e &= \frac{EA}{l_e} \begin{bmatrix} 1 & -1 \\ -1 & 1 \end{bmatrix}, \\ \mathbf{k}^e &= \mathbf{T}_e^T \hat{\mathbf{k}}_e \mathbf{T}_e, \\ \mathbf{m}_e &= \frac{\rho A l_e}{2} \begin{bmatrix} 1 & & & & & \\ & 1 & & & & \\ & & 1 & & & \\ & & & 1 & & \\ & & & & 1 & \\ & & & & & 1 \end{bmatrix}. \end{aligned} \quad (8)$$

where cosines of the members can be expressed in terms of the global coordinates of their ends (Koohestani and Kaveh 2010), and hence transformation matrix will be

$$\mathbf{T}_e = \begin{bmatrix} \cos\theta_x & \cos\theta_y & \cos\theta_z & 0 & 0 & 0 \\ 0 & 0 & 0 & \cos\theta_x & \cos\theta_y & \cos\theta_z \end{bmatrix} \quad (9)$$

Equation of motion is stated as

$$\mathbf{M}\ddot{\mathbf{u}}(t) + \mathbf{C}\dot{\mathbf{u}}(t) + \mathbf{K}\mathbf{u}(t) = \mathbf{P}(t) \quad (10)$$

$\mathbf{M}$ ,  $\mathbf{C}$ ,  $\mathbf{K}$  and  $\mathbf{P}$  indicate mass, damping and stiffness matrices, and loading vector, respectively. Furthermore,  $\ddot{\mathbf{u}}$ ,  $\dot{\mathbf{u}}$  and  $\mathbf{u}$  express acceleration, velocity and displacement vectors, respectively. These vectors are functions of time  $t$  and hereafter are shown without  $t$  for brevity. Eigenvalue problem for structural dynamics can be expressed as

$$\mathbf{K}\boldsymbol{\varphi}_n = \lambda_n \mathbf{M}\boldsymbol{\varphi}_n \quad (11)$$

$\lambda_n$  and  $\boldsymbol{\varphi}_n$  are eigenvalue and the corresponding eigenvector, respectively.

### 3.2 Dynamic analysis of cyclic symmetric structures

Two types of approaches can be used for solving the linearly elastic dynamic equilibrium equation, Eq. (10). The first type consists of direct integration methods like central difference, Wilson-Teta, Newmark-Beta, and so on. These temporal discretization methods solve the coupled system of differential equations such as Eq. (10). The second type solves decoupled form of Eq. (10) using modal analysis, which is also called mode superposition or normal mode method. The decoupled equations can be solved by either Duhamel integration or the aforementioned numerical integration methods (Clough and Penzien 2003) and (Clough 2012). In this paper, modal analysis associated with Newmark-Beta integration technique is utilized.

For an earthquake excitation, the governing equation can be reformed as

$$\mathbf{M}\ddot{\mathbf{u}} + \mathbf{C}\dot{\mathbf{u}} + \mathbf{K}\mathbf{u} = \mathbf{M}\mathbf{r}\ddot{u}_g(t) \quad (12)$$

where from the right hand side of Eq. (12), the minus sign is eliminated. This alteration does not change the problem and only the response sign will be multiplied by -1. However, it can be implemented by minus of earthquake record values,  $\ddot{u}_g(t)$ .  $\mathbf{r}$  is an influence coefficient vector which manifests the displacements resulted from a unit support displacement. As an example,  $\mathbf{r} = \{\mathbf{1}\} \otimes \langle 1 \ 0 \ 0 \rangle^T$  denotes the earthquake excitation at x direction for a 3D truss structure.

In the first step, stiffness matrices should be transformed to cylindrical coordinate system. This transformation may be found in Kaveh and Nematı (2010). Lumped mass matrix is then written as  $\mathbf{M} = \mathbf{I} \otimes \mathbf{A}_M$ , and there is no need to be transformed. After imposing Eq. (3) and Kronecker product properties (see Brewer 1978) about Kronecker products, the eigenvalue problem is derived as

$$\begin{aligned} \mathbf{K}\boldsymbol{\varphi}_i &= \lambda_i \mathbf{M}\boldsymbol{\varphi}_i, \\ (\mathbf{I} \otimes \mathbf{A}_K + \mathbf{H} \otimes \mathbf{B}_K + \mathbf{H}^t \otimes \mathbf{B}_K^T)\boldsymbol{\varphi}_i &= \lambda_i (\mathbf{I} \otimes \mathbf{A}_M)\boldsymbol{\varphi}_i, \\ (\mathbf{I} \otimes \mathbf{A}_M^{-1})(\mathbf{I} \otimes \mathbf{A}_K + \mathbf{H} \otimes \mathbf{B}_K + \mathbf{H}^T \otimes \mathbf{B}_K^T)\boldsymbol{\varphi}_i &= \lambda_i \boldsymbol{\varphi}_i, \\ (\mathbf{I} \otimes \mathbf{A}_M^{-1}\mathbf{A}_K + \mathbf{H} \otimes \mathbf{A}_M^{-1}\mathbf{B}_K + \mathbf{H}^T \otimes \mathbf{A}_M^{-1}\mathbf{B}_K^T)\boldsymbol{\varphi}_i &= \lambda_i \boldsymbol{\varphi}_i. \end{aligned} \quad (13)$$

Therefore, Eq. (6) is converted to

$$eig(\mathbf{K}) = \bigcup_{j=1}^m \left[ eig(\mathbf{A}_M^{-1}(\mathbf{A}_K + \lambda_j \mathbf{B}_K + \bar{\lambda}_j \mathbf{B}_K^T)) \right] \quad (14)$$

Eq. (14) can be used for eigenvalue analysis of block diagonal mass matrix. For purely

diagonal mass matrix, we have  $\mathbf{M} = \mathbf{I} \otimes (m\mathbf{I}_M)$ . Thus

$$\begin{aligned} (\mathbf{I} \otimes \mathbf{A}_K + \mathbf{H} \otimes \mathbf{B}_K + \mathbf{H}^t \otimes \mathbf{B}_K^t) \boldsymbol{\varphi}_i &= \frac{\lambda_i}{m} \boldsymbol{\varphi}_i, \\ \mathbf{K} \boldsymbol{\varphi}_i &= \left( \frac{\lambda_i}{m} \right) \boldsymbol{\varphi}_i. \end{aligned} \quad (15)$$

Though block diagonal mass matrix, Eq. (14), is utilized in this study. The purely diagonal form, Eq. (15) is clearly simpler than the former. An important transformation is also necessary for load vector. Load vector is the multiple of mass matrix and the influence vector. Since mass matrix is expressed in cylindrical coordinate system, the influence vector is transformed by

$$\mathbf{r}_\theta = \mathbf{T}_\theta^T \mathbf{r} \quad (16)$$

in which

$$\mathbf{T}_\theta = \begin{bmatrix} \mathbf{T}^1 & & & & \\ & \ddots & & & \\ & & \mathbf{T}^i & & \\ & & & \ddots & \\ & & & & \mathbf{T}^n \end{bmatrix}, \quad (17)$$

$$\mathbf{T}^i = \begin{bmatrix} \cos \theta_i & -\sin \theta_i & 0 \\ \sin \theta_i & \cos \theta_i & 0 \\ 0 & 0 & 1 \end{bmatrix}.$$

It should be noted that  $\mathbf{T}_\theta$  is a  $3n$  by  $3n$  sparse and block diagonal matrix encountering minimal or sub-minimal computational cost, and  $n$  indicates the number of substructures. Eqs. (5) and (14)-(15) solve eigenvalues and eigenvectors of the problem. The governing equation is rewritten as

$$\mathbf{M}\ddot{\mathbf{u}} + \mathbf{C}\dot{\mathbf{u}} + \mathbf{K}\mathbf{u} = \mathbf{M}\mathbf{T}_\theta^T \mathbf{r}\ddot{u}_g(t) \quad (18)$$

In Eq. (18), the mass, damping and stiffness matrices are expressed in cylindrical coordinate system. However, the notations are remained as before, and indices notations are dropped for briefness. Decoupling the equation by modal vectors yields

$$\mathbf{M}_n \ddot{\mathbf{Y}} + \mathbf{C}_n \dot{\mathbf{Y}} + \mathbf{K}_n \mathbf{Y} = \boldsymbol{\Phi}^T \mathbf{M} \mathbf{T}_\theta^T \mathbf{r} \ddot{u}_g(t) \quad (19)$$

where

$$\begin{aligned}
\mathbf{M}_n &= \mathbf{\Phi}^T \mathbf{M} \mathbf{\Phi} = \begin{bmatrix} M_1 & & \\ & \ddots & \\ & & M_{nm} \end{bmatrix}, \\
\mathbf{K}_n &= \mathbf{\Phi}^T \mathbf{K} \mathbf{\Phi} = \begin{bmatrix} K_1 & & \\ & \ddots & \\ & & K_{nm} \end{bmatrix}, \\
\mathbf{C}_n &= \begin{bmatrix} 2\xi_1 \omega_1 M_1 & & \\ & \ddots & \\ & & 2\xi_{nm} \omega_{nm} M_{nm} \end{bmatrix}
\end{aligned} \tag{20}$$

Where  $\ddot{\mathbf{Y}}$ ,  $\dot{\mathbf{Y}}$  and  $\mathbf{Y}$  denote modal acceleration, velocity and displacement vectors, respectively. Eq. (19) represents decoupled modal equation in cylindrical coordinate system which will here be solved by Newmark-Beta method. If modal matrix is normalized with respect to mass matrix, then  $\mathbf{M}_n$  matrix will be an identity matrix, otherwise,  $\mathbf{M}_n$  matrix should be calculated as previously mentioned.  $nm$  indicates the number of DOFs as all modes are included here. In practice, identical damping ratio,  $\xi$ , is usually considered for all modes leading to  $\xi_i = \xi$ . Since diagonal mass matrix is selected, it is not necessary to transform this type of damping matrix as it is diagonal the same as  $\mathbf{M}_n$ .

Finally, as the displacement response is determined in cylindrical coordinate system, it should be transformed back to the Cartesian coordinate system by

$$\mathbf{u}(t) = \mathbf{T}_\theta \mathbf{\Phi} \mathbf{Y}(t) \tag{21}$$

$\mathbf{u}(t)$  is the displacement response vector at the time  $t$ .

#### 4. Canonical forms for random dynamic analysis

##### 4.1 A concise introduction to random vibration in frequency domain

Random vibration theory is a useful discipline for random dynamic analysis of structures under random loading which particularly involves earthquake, wind, and ocean wave loads, Newland (2012). Here, frequency domain random analysis of a structure subjected to earthquake loading is briefly discussed. Frequency domain counterpart of Eq. (10) is

$$\begin{aligned}
\mathbf{H}(\varpi) \mathbf{U}(\varpi) &= \mathbf{P}(\varpi), \\
\mathbf{H}(\varpi) &= [\mathbf{K} - \varpi^2 \mathbf{M} + i \varpi \mathbf{C}]^{-1}.
\end{aligned} \tag{22}$$

$\mathbf{P}$ ,  $\mathbf{U}$  and  $\mathbf{H}$  are load vector, displacement vector and transfer function matrix, respectively. These are all functions of the frequency  $\varpi$ , and  $i = \sqrt{-1}$  is the complex unit. In order to analyze a structure subjected to random loading using modal data, the challenging equation is expressed as

$$S_{resp.}(\varpi) = \sum_{m=1}^N \sum_{n=1}^N B_m B_n H_m(-i\varpi) H_n(i\varpi) S_{P_m P_n}(\varpi) \quad (23)$$

where

$$H_n(i\varpi) = \frac{1}{M_n [1 + 2i\xi_n \omega_n \varpi - \varpi^2]}, \quad (24)$$

$$H_m(-i\varpi) = \frac{1}{M_m [1 - 2i\xi_m \omega_m \varpi - \varpi^2]}.$$

$H_n$ ,  $M_n$ ,  $\xi_n$ ,  $\omega_n$  are transfer function, mass, damping ratio, natural angular frequency associated with the  $n$ th mode, respectively.  $B_n$  is a coefficient relating the  $n$ th normal coordinate to any desired response quantity.  $S_{P_m P_n}(\varpi)$  is modal load spectral density function.  $S_{resp.}(\varpi)$  is a response spectral density function.  $\varpi$  is a parametric value as a variable in frequency domain.  $N$  is the number of selected modes. The following equation represents variance of response considering a broad band spectral density input

$$\sigma_{resp.}^2(\varpi) = \sum_{m=1}^N \sum_{n=1}^N B_m B_n \left( \int_{-\infty}^{\infty} H_m(-i\varpi) H_n(i\varpi) S_{P_m P_n}(\varpi) d\varpi \right) \quad (25)$$

Suppose that Gaussian random process governs and modal spectral density function matrix is defined by constant white noise value  $S_0$  affected by the influence vector  $\mathbf{r}$ . Obviously,  $S_0$  is spectral density value of seismic excitation considered as a random process. Thus,  $\mathbf{S}_{i_g} = S_0 \mathbf{r} \mathbf{r}^T$  leads to

$$S_{P_m P_n}(\omega) = \boldsymbol{\phi}_m^T \mathbf{M} \mathbf{r} S_0 \mathbf{r}^T \mathbf{M} \boldsymbol{\phi}_n \quad (26)$$

Since damping ratio in commonly used structures is less than 10 per cent (Clough and Penzien 2003), one can neglect the cross terms of Eq. (25) leading to small values, therefore

$$\sigma_{resp.}^2(\omega) = \frac{\pi}{2\xi} \sum_{n=1}^N \frac{B_n^2 S_{P_n P_n}}{M_n^2 \omega_n^3} \quad (27)$$

#### 4.2 Matrices comprising in symmetric structures

Canonical forms for eigensolution of some matrices with well-known patterns exist in literature (Yueh 2005, Kouachi 2006). These analytical solutions were utilized for eigenvalue analysis of symmetric structures by (Kaveh and Rahami 2007). In this subsection, analytical solutions for random vibration analysis of shear frames for two types of 2D and 3D frames are developed. Though more DOFs may be defined for a 3D shear frame, only practical cases are evaluated here.

*Case 1:* For a 2D shear frame, each story has one lateral DOF as indicated in Fig. 1, emphasizing that for a shear frame with identical mass ( $m$ ) and stiffness ( $k_0$ ) at every story, mass and stiffness matrices are in the following forms, respectively



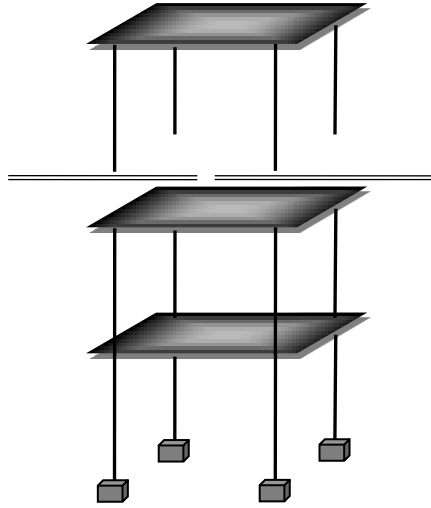


Fig. 2 A  $ns$  story 3D shear frame

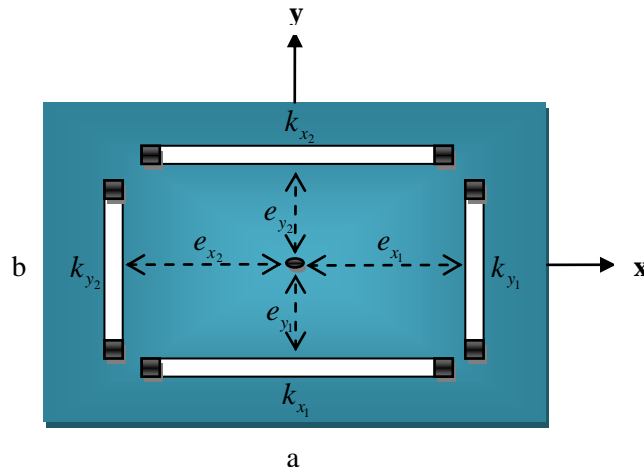


Fig. 3 A typical story template of the 3D shear frame

$$\mathbf{K}^e = \begin{bmatrix} \mathbf{k}^e & -\mathbf{k}^e \\ -\mathbf{k}^e & \mathbf{k}^e \end{bmatrix} \quad (31)$$

After imposing the support conditions, the assembled stiffness matrix will be obtained as

Table 1 Comparison of natural frequencies solved by the two methods for the truss structure	
	Natural frequencies (Rad/sec)
Standard method	[720.1572, 720.1572, 927.1593, ... , 2426.51, 2797.37, 2797.37]
Graph product method	[720.1572, 720.1572, 927.1593, ... , 2426.51, 2797.37, 2797.37]



### 5.1 Example 1: Time history analysis of a 3D truss

Static analysis of the truss shown in Fig. 4 had been performed by employing graph product rules in Kaveh and Rahami (2010), by employing graph product rules. Here, the graph product based method developed in Section 3 is employed for dynamic analysis. Time history analysis of this structure under El Centro earthquake excitation, Fig. 5, is accomplished using a time interval of 0.02 sec. Damping ratio for all the modes is taken as 5 per cent. Material elasticity and density are  $2 \times 10^8$  kN/m<sup>2</sup> and 7.58 kNs<sup>2</sup>/m, respectively. All the cross sectional areas are considered as 5 cm<sup>2</sup>. The structure is formed by strong Cartesian product of the path  $P_2$  and the cycle  $C_5$ . Indeed, the structure is constructed by two equilateral polygons with five edges. The circumscribed circles of the polygons have radiuses as 1.5 and 3 m. Forming the structural matrices in cylindrical coordinates system as described in Section 3 results in

$$\begin{aligned}
 \mathbf{A}_M &= \begin{bmatrix} 23.9346 & 0 & 0 \\ 0 & 23.9346 & 0 \\ 0 & 0 & 23.9346 \end{bmatrix}, \\
 \mathbf{A}_K &= 10^8 \times \begin{bmatrix} 0.6463 & 0 & -0.1867 \\ 0 & 1.2063 & 0 \\ -0.1867 & 0 & 0.3639 \end{bmatrix}, \\
 \mathbf{B}_K &= 10^7 \times \begin{bmatrix} 1.9593 & -2.6967 & 0 \\ 2.6967 & -3.7117 & 0 \\ 0 & 0 & 0 \end{bmatrix}.
 \end{aligned} \tag{36}$$

Table 2 Displacement maxima of the truss's top nodes acquired by the two methods

Node number	Standard method			Graph product method		
	$x$	$y$	$z$	$x$	$y$	$z$
2	2.4368E-06	6.0238E-09	8.6265E-09	2.4369E-06	1.0921E-21	1.1062E-21
4	3.0020E-06	1.8346E-07	1.4800E-06	3.0020E-06	1.8362E-07	1.4799E-06
6	2.6527E-06	2.3148E-07	9.1436E-07	2.6527E-06	2.3126E-07	9.1461E-07
8	2.6527E-06	2.9697E-07	7.3756E-07	2.6527E-06	2.9711E-07	7.3791E-07
10	3.0020E-06	1.4316E-07	1.1941E-06	3.0020E-06	1.4292E-07	1.1940E-06

Table 3 Displacement minima of the truss's top nodes acquired by the two methods

Node number	Standard method			Graph product method		
	$x$	$y$	$z$	$x$	$y$	$z$
2	-1.8307E-06	-6.0882E-09	-8.6886E-09	-1.8307E-06	-1.1210E-21	-1.6402E-21
4	-2.2706E-06	-1.4269E-07	-1.1938E-06	-2.2705E-06	-1.4292E-07	-1.1940E-06
6	-1.9987E-06	-2.9725E-07	-7.3826E-07	-1.9987E-06	-2.9711E-07	-7.3791E-07
8	-1.9987E-06	-2.3103E-07	-9.1488E-07	-1.9987E-06	-2.3126E-07	-9.1461E-07
10	-2.2706E-06	-1.8379E-07	-1.4798E-06	-2.2705E-06	-1.8362E-07	-1.4799E-06

Natural angular frequencies of the structure for three lowest and highest modes obtained by standard method and the method based on Eqs. (14) or (15) are compared in Table 1. Also, Tables 2 and 3 compare the maximum and minimum displacements of top nodes for both methods. Since earthquake excitation is assumed to be at  $x$  direction, it is visible that the response error is minimal

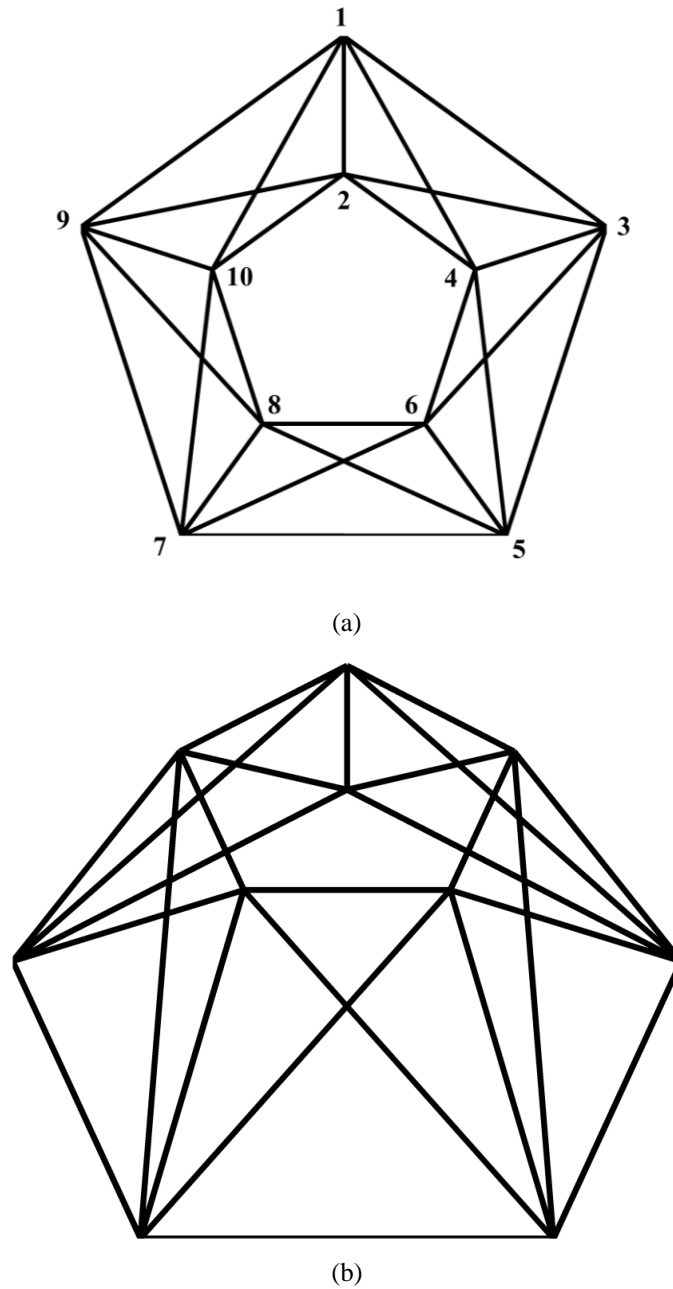


Fig. 4 A truss structure generated by graph product: (a) plan view with nodal numbering, (b) isometric view

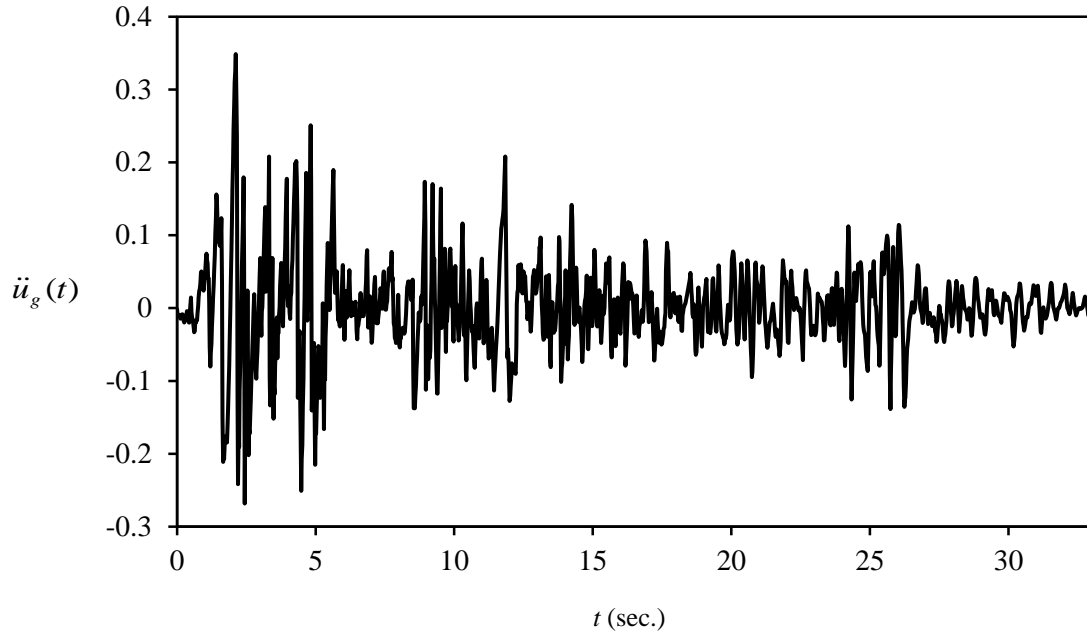


Fig. 5 El Centro (N-S component, 1940) earthquake accelerogram ( $\ddot{u}_g(t)$  in g unit)

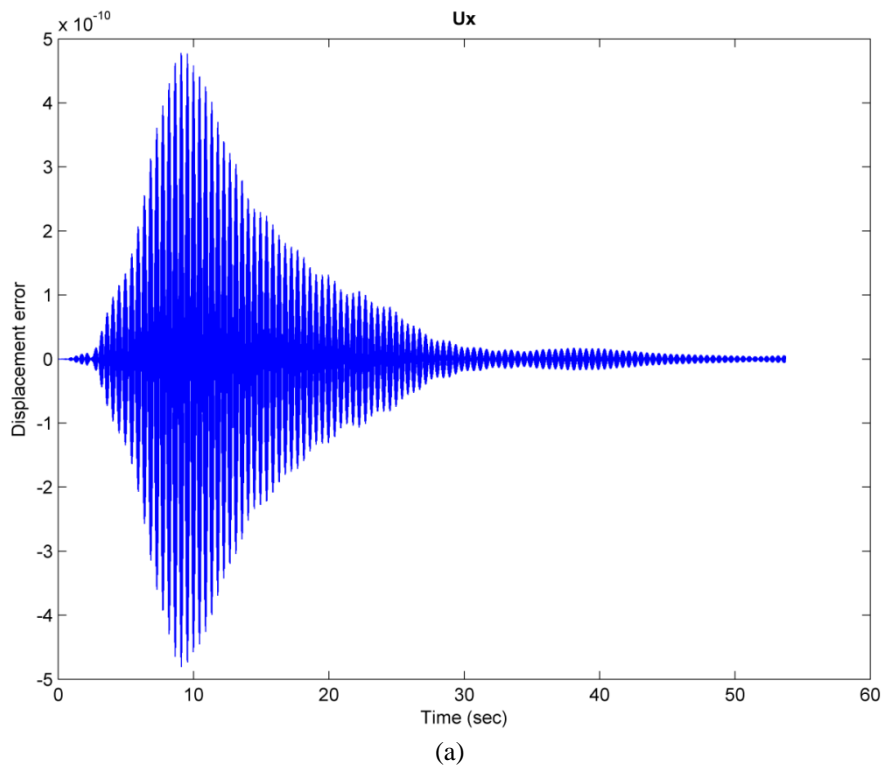


Fig. 6 Displacement error history of the node 2 of the truss structure: (a) at  $x$  direction, and (b) at  $y$  direction and (c) at  $z$  direction

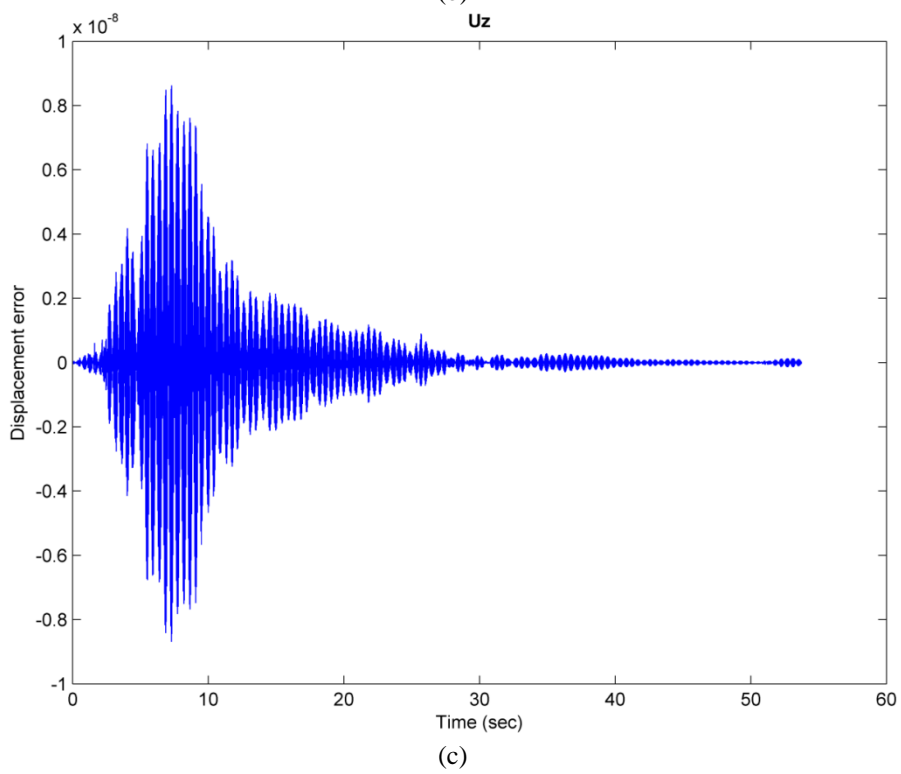
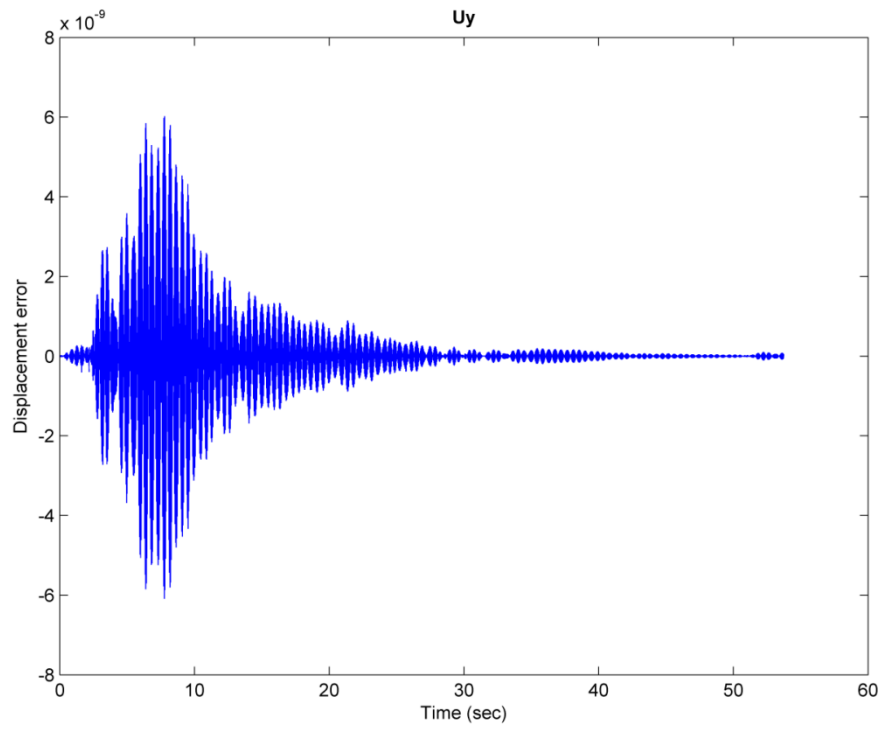


Fig. 6 Continued

with respect to other directions. Though displacement responses of the presented method at the excitation direction (e.g., here is  $x$ ) have desirable accuracy, sometimes responses at other directions (i.e.,  $y$  and  $z$ ) have large errors compared to their standard counterpart methods. Nonetheless, the target is usually the displacement at the direction which is excited. As a sample, error displacement response history for node 2 is represented in Fig. 6. This error history is obtained by response differences of two methods as  $R_{GP} - R_S$ ;  $R_{GP}$  and  $R_S$  denote the graph product based method response and standard method response, respectively. It is apparent that accuracy order of error history is acceptable with respect to accuracy order of the extremum (minima/maxima) values as provided by Tables 2 and 3, particularly for  $x$  direction which the structure is excited. For instance, node 2 has maximum  $2.4368 \times 10^{-6}$  m displacement at  $x$  direction, whereas Fig. 6(a) illustrates the response error maxima with an order of  $5 \times 10^{-10}$ .

### 5.2 Example 2: Time history analysis of a space dome

In this example, the presented graph product based method is utilized for time history analysis of a dome structure, shown in Fig. 7, under the El Centro accelerogram. This structure is formed by strong Cartesian product of two graph generators  $P_8$  by  $C_{24}$ . The radius of the dome at the lowest part and the highest part are 14 and 7.5 m, respectively. Table 4 discloses the cylindrical coordinates of a path graph generator. The cross sectional areas are taken as  $20 \text{ cm}^2$ . All the ground level nodes are simply supported. The accelerogram are equally imposed to the structure at all three directions. Other structural and loading properties are the same as those of Example 1.

The structural matrices casted in cylindrical coordinates as explained in Section 3, provide an efficient analysis utilizing  $\mathbf{A}_M$ ,  $\mathbf{A}_K$  and  $\mathbf{B}_K$ . Nevertheless, these are obviously different regarding to the previous structure. For example,  $\mathbf{A}_M$  has not identical diagonal terms as already calculated in the Example 1 and it relies on topological properties of the structure (i.e., structural connectivity). Natural angular frequencies of the dome attained by standard method and presented method are compared in Table 5 involving six lowest and highest modes' frequencies. Furthermore, Tables 6 and 7 compare the maximum and minimum displacements of the top nodes for both methods, and error displacement response history for the node 24 is displayed in Fig. 8. Note that nodal numbering is assigned as in Example 1. In contrast to the Example 1, an important point is that in the case when the structure is simultaneously excited at all directions, the errors in all directions are minimal, and leads to a suitable accuracy as demonstrated by Fig. 8. As an

Table 4 Cylindrical coordinates of a generator of the dome and its nodal numbering

Node number	$r$ (m)	$\theta$ (Deg)	$z$ (m)
1	14	0	0
2	13	0	1.5
3	11	0	3.5
4	9	0	5
5	7	0	6
6	5	0	6.75
7	3	0	7.25
8	1	0	7.5

example, Table 6 reveals that the maximum displacements of node 24 are  $1.92 \times 10^{-4}$ ,  $1.87 \times 10^{-4}$  and  $3.11 \times 10^{-4}$  m at  $x$ ,  $y$  and  $z$  directions, respectively. While Fig. 8 indicates that the maxima or minima error (i.e., response difference histories) have an order of  $1.5 \times 10^{-6}$ ,  $1.5 \times 10^{-6}$ ,  $5 \times 10^{-7}$  at  $x$ ,  $y$  and  $z$  directions, respectively.

Table 5 Comparison of natural frequencies solved by the two methods for the dome structure

Natural frequencies (Rad/sec)	
Standard Method	[0.000241, 0.000275, 0.000292, 0.000325, 0.00036, 0.00042, ... , 9980.702, 10419.81, 10419.81, 10686.66, 10686.66, 10776.17]
Graph product method	[0.000221, 0.000243, 0.000243, 0.000318, 0.000318, 0.000501, ... , 9980.702, 10419.81, 10419.81, 10686.66, 10686.66, 10776.17]

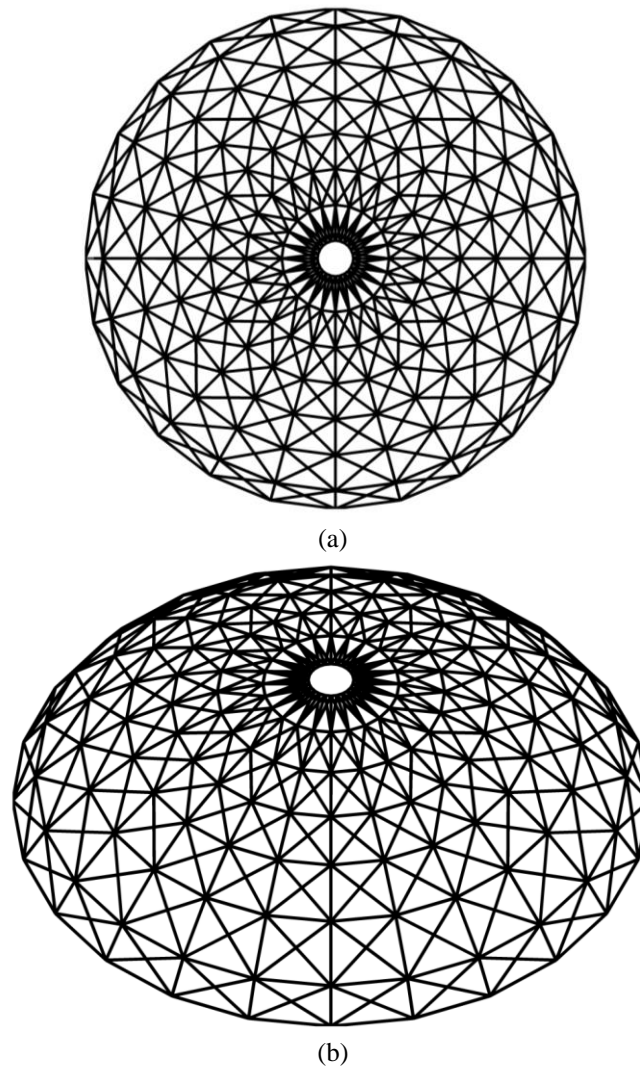


Fig. 7 A dome structure generated by graph product: (a) plan view, and (b) isometric view

Table 6 Displacement maxima of the dome's top nodes acquired by the two methods

Node number	Standard method			Graph product method		
	$x$	$y$	$z$	$x$	$y$	$z$
8	0.000193	0.000181	0.000298	0.000193	0.000181	0.000298
16	0.000193	0.000184	0.000306	0.000193	0.000184	0.000306
24	0.000192	0.000187	0.000311	0.000192	0.000187	0.000311
32	0.00019	0.00019	0.000312	0.00019	0.00019	0.000312
40	0.000187	0.000192	0.000311	0.000187	0.000192	0.000311
48	0.000184	0.000193	0.000306	0.000184	0.000193	0.000306
56	0.000181	0.000193	0.000298	0.000181	0.000193	0.000298
64	0.000177	0.000192	0.000288	0.000178	0.000192	0.000288
72	0.000175	0.000191	0.000277	0.000175	0.000191	0.000277
80	0.000173	0.000188	0.000264	0.000173	0.000188	0.000264
88	0.000172	0.000186	0.000252	0.000172	0.000186	0.000252
96	0.000171	0.000183	0.00024	0.000171	0.000183	0.00024
104	0.000171	0.000181	0.00023	0.000171	0.000181	0.00023
112	0.000172	0.000178	0.000224	0.000172	0.000178	0.000224
120	0.000173	0.000176	0.000226	0.000173	0.000176	0.000225
128	0.000174	0.000174	0.000226	0.000175	0.000175	0.000226
136	0.000176	0.000173	0.000226	0.000176	0.000173	0.000225
144	0.000178	0.000172	0.000224	0.000178	0.000172	0.000224
152	0.000181	0.000171	0.00023	0.000181	0.000171	0.00023
160	0.000183	0.000171	0.00024	0.000183	0.000171	0.00024
168	0.000186	0.000172	0.000252	0.000186	0.000172	0.000252
176	0.000188	0.000173	0.000264	0.000188	0.000173	0.000264
184	0.000191	0.000175	0.000277	0.000191	0.000175	0.000277
192	0.000192	0.000177	0.000288	0.000192	0.000178	0.000288

Table 7 Displacement minima of the dome's top nodes acquired by the two methods

Node number	Standard method			Graph product method		
	$x$	$y$	$z$	$x$	$y$	$z$
8	-0.00024	-0.00022	-0.00033	-0.00024	-0.00022	-0.00033
16	-0.00024	-0.00023	-0.00034	-0.00024	-0.00023	-0.00034
24	-0.00023	-0.00023	-0.00035	-0.00023	-0.00023	-0.00035
32	-0.00023	-0.00023	-0.00035	-0.00023	-0.00023	-0.00035
40	-0.00023	-0.00023	-0.00035	-0.00023	-0.00023	-0.00035
48	-0.00023	-0.00024	-0.00034	-0.00023	-0.00024	-0.00034
56	-0.00022	-0.00024	-0.00033	-0.00022	-0.00024	-0.00033
64	-0.00022	-0.00023	-0.00031	-0.00022	-0.00023	-0.00032
72	-0.00022	-0.00023	-0.0003	-0.00022	-0.00023	-0.0003
80	-0.00021	-0.00023	-0.00029	-0.00021	-0.00023	-0.00029

Table 7 Continued

Node number	Standard method			Graph product method		
	x	y	z	x	y	z
88	-0.00021	-0.00023	-0.00028	-0.00021	-0.00023	-0.00028
96	-0.00021	-0.00022	-0.00027	-0.00021	-0.00022	-0.00027
104	-0.00021	-0.00022	-0.00026	-0.00021	-0.00022	-0.00026
112	-0.00021	-0.00022	-0.00025	-0.00021	-0.00022	-0.00025
120	-0.00021	-0.00022	-0.00024	-0.00022	-0.00022	-0.00024
128	-0.00022	-0.00022	-0.00024	-0.00022	-0.00022	-0.00024
136	-0.00022	-0.00021	-0.00024	-0.00022	-0.00022	-0.00024
144	-0.00022	-0.00021	-0.00025	-0.00022	-0.00021	-0.00025
152	-0.00022	-0.00021	-0.00026	-0.00022	-0.00021	-0.00026
160	-0.00022	-0.00021	-0.00027	-0.00022	-0.00021	-0.00027
168	-0.00023	-0.00021	-0.00028	-0.00023	-0.00021	-0.00028
176	-0.00023	-0.00021	-0.00029	-0.00023	-0.00021	-0.00029
184	-0.00023	-0.00022	-0.0003	-0.00023	-0.00022	-0.0003
192	-0.00023	-0.00022	-0.00031	-0.00023	-0.00022	-0.00032

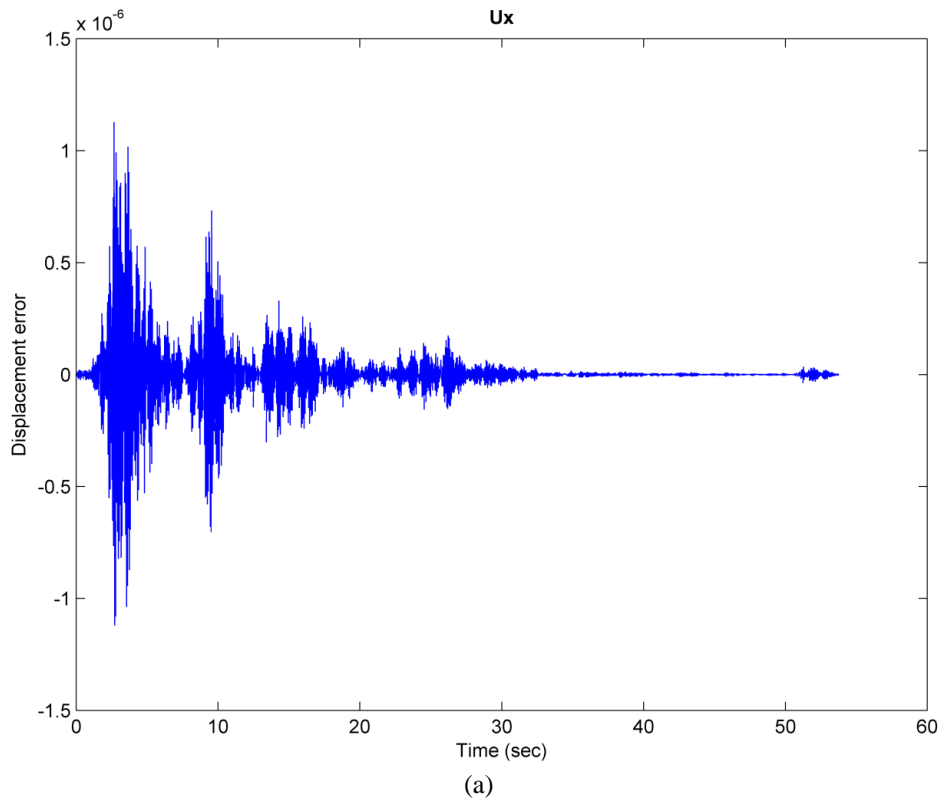
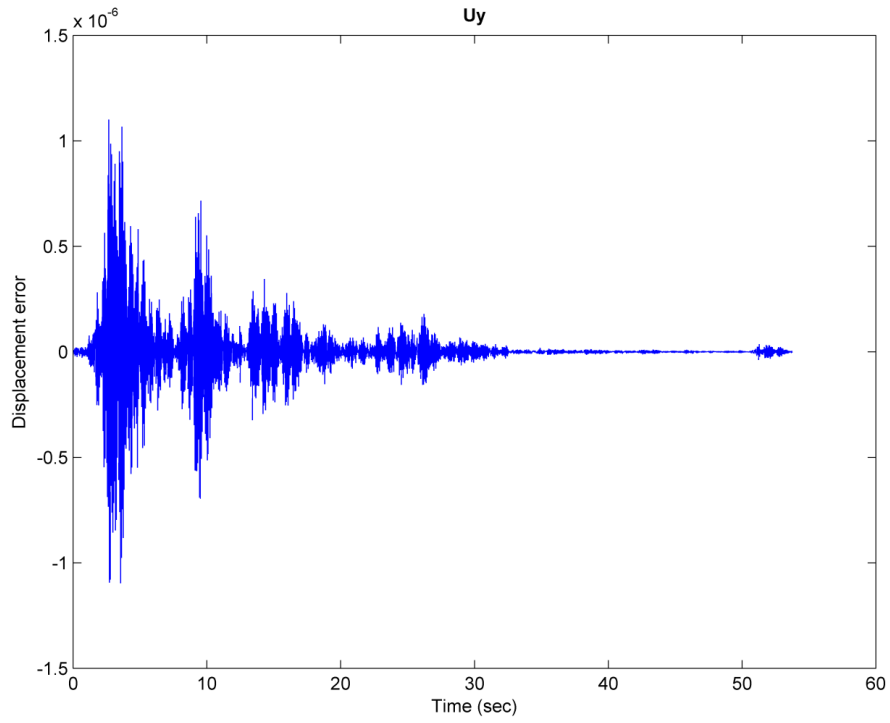
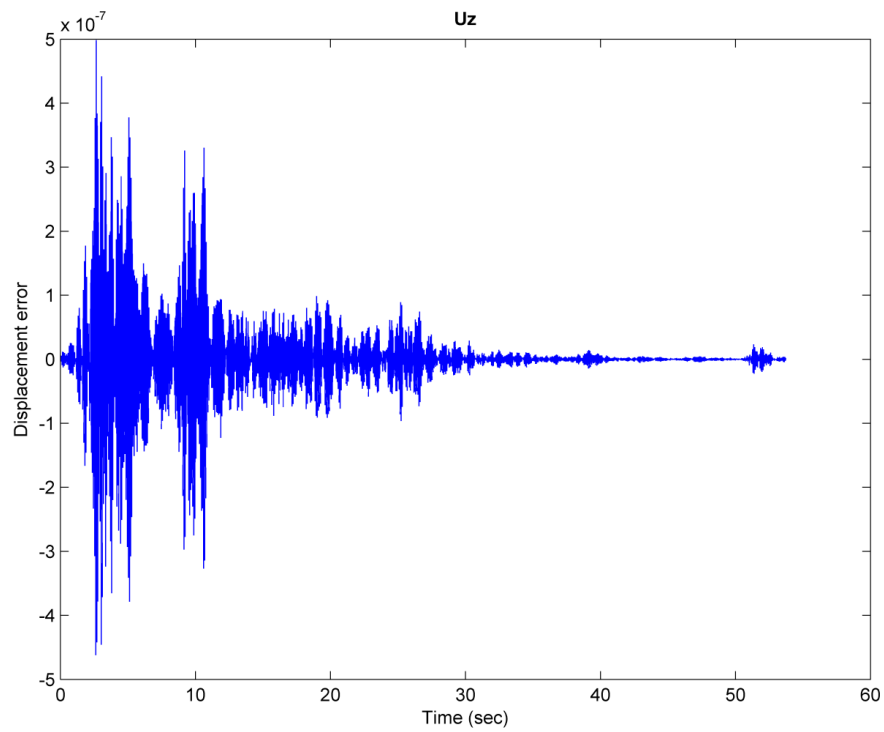


Fig. 8 Displacement error history of the node 24 of the dome structure: (a) at x direction, and (b) at y direction and (c) at z direction



(b)



(c)

Fig. 8 Continued

### 5.3 Example 3: A 2D shear frame excited by random seismic load

Here, a 2D shear frame is subjected to random seismic loading. Random analysis is performed in frequency domain and spectral density function of seismic input is assumed to be constant broad band white noise  $S_0$  affected by the influence vector. The remaining assumptions are mentioned in the previous section. Firstly, eigenvalues and eigenvectors are obtained as follows:

Using the relation presented in Yueh (2005), Kronecker product properties provided in Brewer (1978), and some mathematical elaborations, we obtain

$$\begin{aligned}\omega_i^2 &= \frac{4k_0}{m} \cos^2\left(\frac{(ns-i+1)\pi}{2ns+1}\right), \\ \phi_i &= \sin\left(\frac{k(2i-1)\pi}{2ns+1}\right) \quad k=1,2,\dots,ns\end{aligned}\quad (37)$$

Secondly,  $B_n$  for target responses are computed as

Base shear

$$B_n = \langle 1, 1, \dots, 1 \rangle_{1 \times ns} \omega_n^2 \mathbf{M} \boldsymbol{\phi}_n \quad (38)$$

That is equal to

$$\begin{aligned}B_n &= \langle 1 \quad \dots \quad 1 \rangle \omega_n^2 (m\mathbf{I}) \boldsymbol{\phi}_n = m \omega_n^2 \text{sum}(\boldsymbol{\phi}_n) \\ &= 4k \cos^2\left(\frac{(ns-n+1)\pi}{2ns+1}\right) \sum_{k=1}^{ns} \sin\left(\frac{k(2n-1)\pi}{2ns+1}\right)\end{aligned}\quad (39)$$

Base moment

$$B_n = \langle h_1, h_2, \dots, h_{ns} \rangle_{1 \times ns} \omega_n^2 \mathbf{M} \boldsymbol{\phi}_n \quad (40)$$

If identical height is taken for every story, then we will have

$$\begin{aligned}B_n &= h \langle 1 \quad 2 \quad \dots \quad ns \rangle \omega_n^2 (m\mathbf{I}) \boldsymbol{\phi}_n \\ &= 4kh \cos^2\left(\frac{(ns-n+1)\pi}{2ns+1}\right) \sum_{k=1}^{ns} k \sin\left(\frac{k(2n-1)\pi}{2ns+1}\right)\end{aligned}\quad (41)$$

$ns$  and  $n$  are the number of stories and mode number, respectively. Spectral density function of earthquake loading is derived as follows

$$\begin{aligned}S_{p_m p_n}(\omega) &= S_0 \boldsymbol{\phi}_m^T m \mathbf{I} \{ \mathbf{1} \} \{ \mathbf{1} \} m \mathbf{I} \boldsymbol{\phi}_n \\ &= S_0 m^2 \text{sum}(\boldsymbol{\phi}_m) \text{sum}(\boldsymbol{\phi}_n)\end{aligned}\quad (42)$$

$\text{sum}(\cdot)$  denotes the sum of the vector entries. Therefore, analytical solution of the base shear and moment variances for this shear frame yields

$$\sigma_V^2 = S_0 m^2 \frac{\pi}{\xi} \sqrt{\frac{k_0}{m} \sum_{n=1}^{ns} \frac{\cos\left(\frac{(ns-n+1)\pi}{2ns+1}\right) \left(\sum_{k=1}^{ns} \sin\left(\frac{k(2n-1)\pi}{2ns+1}\right)\right)^4}{\left(\sum_{k=1}^{ns} \sin^2\left(\frac{k(2n-1)\pi}{2ns+1}\right)\right)^2}} \quad (43)$$

Table 8 Results of random vibration analyses for 2D shear frame (Example 3)

	Standard method	Present method
Natural frequencies	$\sqrt{\frac{k}{m}}$ [0.0156, 0.0469, 0.0781, 0.1094, ..., 1.9961, 1.9978, 1.9990, 1.9998]	$\sqrt{\frac{k}{m}}$ [0.0156, 0.0469, 0.0781, 0.1094, ..., 1.9961, 1.9978, 1.9990, 1.9998]
Base shear force variance	$54.532091154012080 \frac{S_0 m^2 \pi}{\xi} \sqrt{\frac{k}{m}}$	$54.532091153985000 \frac{S_0 m^2 \pi}{\xi} \sqrt{\frac{k}{m}}$
	2.132340771817836e+05	2.132340771816758e+05
Base moment variance	$\frac{S_0 m^2 h^2 \pi}{\xi} \sqrt{\frac{k}{m}}$	$\frac{S_0 m^2 h^2 \pi}{\xi} \sqrt{\frac{k}{m}}$

Table 9 All relevant parameters chosen for 3D shear frame (Example 4)

Variable	Assigned value
Plane dimensions	a=2b=6
Story height	h=3.5
Stiffness at x direction	$k_{x_1} = 2k_{x_2} = 2k_0$
Stiffness at y direction	$2k_{y_1} = 3k_{y_2} = 6k_0$
Eccentricity at x direction	$2e_{x_1} = 4e_{x_2} = 2b$
Eccentricity at y direction	$2e_{y_1} = 2e_{y_2} = b$
Lumped masses at each floor	m and $I_o = 3.75m$

$$\sigma_M^2 = S_0 m^2 h^2 \frac{\pi}{\xi} \sqrt{\frac{k_0}{m}} \sum_{n=1}^{ns} \frac{\cos\left(\frac{(ns-n+1)\pi}{2ns+1}\right) \left(\sum_{k=1}^{ns} k \sin\left(\frac{k(2n-1)\pi}{2ns+1}\right)\right)^2 \left(\sum_{k=1}^{ns} \sin\left(\frac{k(2n-1)\pi}{2ns+1}\right)\right)^2}{\left(\sum_{k=1}^{ns} \sin^2\left(\frac{k(2n-1)\pi}{2ns+1}\right)\right)^2} \quad (44)$$

Natural frequencies, variances of base shear force and moment for a 100-story shear frame are listed in Table 8 and compared to the standard procedure. The outcomes exhibit good agreement between the two methods. Evidently, Eqs. (43) and (44) solve the problem with minimal computational effort.

#### 5.4 Example 4: A 3D shear frame excited by random seismic load

This example presents a formulation for random vibration analysis of a 3D shear building in frequency domain using canonical forms. Eigenvalue problem, Eq. (11), for the mentioned structure is simplified as follows:

According to the Kronecker product rules (Brewer 1978), when Eq. (35) is substituted in Eq. (11) we obtain

$$\begin{aligned}
\mathbf{N} \otimes \mathbf{k}^e \boldsymbol{\varphi}_i &= \lambda_i \mathbf{I} \otimes \mathbf{m}^e \boldsymbol{\varphi}_i \\
(\mathbf{I}^{-1} \otimes \mathbf{m}^{e-1})(\mathbf{N} \otimes \mathbf{k}^e) \boldsymbol{\varphi}_i &= \lambda_i \boldsymbol{\varphi}_i, \\
(\mathbf{I}^{-1} \mathbf{N}) \otimes (\mathbf{m}^{e-1} \mathbf{k}^e) \boldsymbol{\varphi}_i &= \lambda_i \boldsymbol{\varphi}_i.
\end{aligned} \tag{45}$$

Hence, the following problem can readily be handled for random vibration analysis

$$\mathbf{N} \otimes (\mathbf{m}^{e-1} \mathbf{k}^e) \boldsymbol{\varphi}_i = \lambda_i \boldsymbol{\varphi}_i. \tag{46}$$

Eigenvalues and eigenvectors are swiftly attained by

$$\begin{aligned}
\lambda_i &= \text{eig}_j(\mathbf{N}) \times \text{eig}_l(\mathbf{m}^{e-1} \mathbf{k}^e), \\
\boldsymbol{\varphi}_i &= \text{eigvec}_j(\mathbf{N}) \otimes \text{eigvec}_l(\mathbf{m}^{e-1} \mathbf{k}^e).
\end{aligned} \tag{47}$$

Analytical eigensolution of  $\mathbf{N}$  matrix is available in Yueh (2005)), therefore, one may write

$$\begin{aligned}
\lambda_i &= [2 + 2 \cos(\frac{2(ns-j+1)\pi}{2ns+1})] \times \text{eig}_l(\mathbf{m}^{e-1} \mathbf{k}^e), \quad j=1,2,\dots, ns, \quad l=1,2,3, \\
\boldsymbol{\varphi}_i &= \sin(\frac{k(2j-1)\pi}{2ns+1}) \otimes \text{eigvec}_l(\mathbf{m}^{e-1} \mathbf{k}^e) = \mathbf{u}^i \otimes \mathbf{v}^i, \quad k=1,2,\dots, ns.
\end{aligned} \tag{48}$$

Consider a 100-story shear frame under a white noise seismic random excitation at horizontal directions defined by

$$\begin{aligned}
\mathbf{S}_{\ddot{u}_g}(\omega) &= S_0 \mathbf{r} \mathbf{r}^T, \\
\mathbf{r}^T &= \langle \mathbf{1} \rangle \otimes \langle 1 \ 0.5 \ 0 \rangle.
\end{aligned} \tag{49}$$

Cross terms of ground acceleration spectral density matrix are zero, when the excitations at  $x$  and  $y$  directions are assumed to be statistically independent. Here,  $\mathbf{S}_{\ddot{u}_g}$  matrix is considered as a function of  $S_0$  and  $\mathbf{r}$ . Therefore, the calculated cross terms will stay unaltered as usual. Table 9 provides the structural properties of this example.

The matrices  $\mathbf{m}^e$  and  $\mathbf{k}^e$  are calculated as follows

$$\mathbf{k}^e = k_0 \begin{bmatrix} 3 & 0 & 1.5 \\ 0 & 5 & 6 \\ 1.5 & 6 & 38.25 \end{bmatrix}, \quad \mathbf{m}^e = m \begin{bmatrix} 1 & 0 & 0 \\ 0 & 1 & 0 \\ 0 & 0 & 3.75 \end{bmatrix}. \tag{50}$$

Eigenvalues and eigenvectors of  $\mathbf{m}^{e-1} \mathbf{k}^e$  are computed as

$$\begin{aligned}
\text{eig}(\mathbf{m}^{e-1} \mathbf{k}^e) &= \frac{k_0}{m} [11.7015, 2.8020, 3.6965], \\
\text{eigvec}(\mathbf{m}^{e-1} \mathbf{k}^e) &= \begin{bmatrix} -0.1274 & -0.9336 & 0.4158 \\ -0.6616 & -0.3364 & -0.8887 \\ -0.7390 & 0.1232 & 0.1931 \end{bmatrix}.
\end{aligned} \tag{51}$$

As an examination, using Eq. (48) leads to the following fundamental angular frequency and corresponding eigenvector

$$\begin{aligned}\omega_{\min}^2 &= [2 + 2 \cos(\frac{200\pi}{201})] \times 2.8020 \frac{k_0}{m} = 0.0007 \frac{k_0}{m} \\ \phi^T &= \sin(\frac{k\pi}{41}) \otimes \text{eigvec}_2(\mathbf{m}^e \mathbf{k}^e) = \dots \\ &[-0.0146 \quad -0.0053 \quad 0.0019 \quad \dots \quad -0.9336 \quad -0.3364 \quad 0.1232]\end{aligned}\quad (52)$$

It should be noted that the eigenvectors determined by this method are inherently not normalized. Since in dynamic analysis of structures these are often normalized with respect to mass matrix; it can conveniently be normalized as

$$\begin{aligned}\hat{\Phi}_n &= \frac{\Phi_n}{\sqrt{M_n}} = \frac{\Phi_n}{\sqrt{\Phi_n^T \mathbf{M} \Phi_n}} = \frac{\mathbf{u}^n \otimes \mathbf{v}^n}{\sqrt{(\mathbf{u}^n)^T \otimes (\mathbf{v}^n)^T (\mathbf{I} \otimes \mathbf{m}^e) (\mathbf{u}^n \otimes \mathbf{v}^n)}} \\ &= \frac{\mathbf{u}^n \otimes \mathbf{v}^n}{\sqrt{(\mathbf{u}^n)^T \mathbf{u}^n \otimes (\mathbf{v}^n)^T \mathbf{m}^e \mathbf{v}^n}} = \frac{\mathbf{u}^n \otimes \mathbf{v}^n}{\|\mathbf{u}^n\| \sqrt{(\mathbf{v}^n)^T \mathbf{m}^e \mathbf{v}^n}}\end{aligned}\quad (53)$$

Using Eqs. (26) and (49) leads to

$$S_{P_m P_n}(\omega) = S_0 \Phi_m^T \mathbf{I} \otimes \mathbf{m}^e \{ \mathbf{1} \} \otimes \begin{Bmatrix} 1 \\ 0.5 \\ 0 \end{Bmatrix} \langle \mathbf{1} \rangle \otimes \langle 1 \quad 0.5 \quad 0 \rangle \mathbf{I} \otimes \mathbf{m}^e \Phi_n \quad (54)$$

By recalling  $\phi_i = \mathbf{u}^i \otimes \mathbf{v}^i$ , we will have

$$S_{P_m P_n}(\omega) = S_0 m^2 \text{sum}(\mathbf{u}^m) \text{sum}(\mathbf{u}^n) (\mathbf{v}^m)^T \begin{Bmatrix} 1 \\ 0.5 \\ 0 \end{Bmatrix} \langle 1 \quad 0.5 \quad 0 \rangle \mathbf{v}^n \quad (55)$$

where

$$\text{sum}(\mathbf{u}^m) = \sum_{k=1}^{ns} \sin(\frac{k(2j-1)\pi}{2ns+1}) \quad (56)$$

Response variances consisting of base shears, base torsion and base moments are obtained using the following  $B_n$  coefficients

Base shear at  $x$  direction

$$\begin{aligned}B_n &= \langle 1 \quad \dots \quad 1 \rangle \otimes \langle 1 \quad 0 \quad 0 \rangle \omega_n^2 (\mathbf{I} \otimes \mathbf{m}^e) (\mathbf{u}^n \otimes \mathbf{v}^n) \\ &= \omega_n^2 \langle 1 \quad \dots \quad 1 \rangle \otimes \langle 1 \quad 0 \quad 0 \rangle \mathbf{u}^n \otimes \mathbf{m}^e \mathbf{v}^n \\ &= m \omega_n^2 \text{sum}(\mathbf{u}^n) \langle 1 \quad 0 \quad 0 \rangle \mathbf{v}^n\end{aligned}\quad (57)$$

Base shear at  $y$  direction

$$B_n = m \omega_n^2 \text{sum}(\mathbf{u}^n) \langle 0 \quad 1 \quad 0 \rangle \mathbf{v}^n \quad (58)$$

Base torsion

$$B_n = m\omega_n^2 \text{sum}(\mathbf{u}^n) \langle 0 \ 0 \ 1 \rangle \mathbf{v}^n \quad (59)$$

Base moment at y direction

$$\begin{aligned} B_n &= h \langle 1 \ 2 \ \dots \ ns \rangle \otimes \langle 1 \ 0 \ 0 \rangle \omega_n^2 (\mathbf{I} \otimes \mathbf{m}^e) (\mathbf{u}^n \otimes \mathbf{v}^n) \\ &= mh\omega_n^2 \langle 1 \ 2 \ \dots \ ns \rangle \mathbf{u}^n \langle 1 \ 0 \ 0 \rangle \mathbf{v}^n \\ &= mh\omega_n^2 \left[ \sum_{k=1}^{ns} k \sin\left(\frac{k(2j-1)\pi}{2ns+1}\right) \right] \langle 1 \ 0 \ 0 \rangle \mathbf{v}^n \end{aligned} \quad (60)$$

Base moment at x direction

$$B_n = mh\omega_n^2 \left[ \sum_{k=1}^{ns} k \sin\left(\frac{k(2j-1)\pi}{2ns+1}\right) \right] \langle 0 \ 1 \ 0 \rangle \mathbf{v}^n \quad (61)$$

Employing Eq. (27) and Eqs. (55)-(61), the demand response variances are determined. Natural frequencies, variances of base shear forces, torsion, and moments for the 100 story 3D shear frame

Table 10 Results of random vibration analyses for 3D shear frame (Example 4)

	Standard method	Present method
Natural frequencies	$\sqrt{\frac{k_0}{m}}$ [0.0262, 0.0301, 0.0535, 0.0785, ..., 6.8281, 6.8340, 6.8381, 6.8406]	$\sqrt{\frac{k_0}{m}}$ [0.0262, 0.0301, 0.0535, 0.0785, ..., 6.8281, 6.8340, 6.8381, 6.8406]
	89.117471500495000	89.118034107036660
Base shear at x direction	$\frac{S_0 m^2 \pi}{\xi} \sqrt{\frac{k_0}{m}}$	$\frac{S_0 m^2 \pi}{\xi} \sqrt{\frac{k_0}{m}}$
	14.349778025196208	14.350105629549597
Base shear at y direction	$\frac{S_0 m^2 \pi}{\xi} \sqrt{\frac{k_0}{m}}$	$\frac{S_0 m^2 \pi}{\xi} \sqrt{\frac{k_0}{m}}$
	69.890507647456200	69.895119287606560
Base torsion	$\frac{S_0 m^2 \pi}{\xi} \sqrt{\frac{k_0}{m}}$	$\frac{S_0 m^2 \pi}{\xi} \sqrt{\frac{k_0}{m}}$
	4.268803313368735e+06	4.268803316933907e+06
Base moment according to y direction	$\frac{S_0 m^2 \pi}{\xi} \sqrt{\frac{k_0}{m}}$	$\frac{S_0 m^2 \pi}{\xi} \sqrt{\frac{k_0}{m}}$
	6.873780220164512e+05	6.873780276189527e+05
Base moment according to x direction	$\frac{S_0 m^2 \pi}{\xi} \sqrt{\frac{k_0}{m}}$	$\frac{S_0 m^2 \pi}{\xi} \sqrt{\frac{k_0}{m}}$

are provided in Table 10 and compared with standard method. This result demonstrates the advantageous and accuracy of the presented method for optimal analysis.

## 6. Conclusions

In this article, graph product rules are applied to dynamic analysis of regular skeletal structures. Here, the formulation of time history dynamic analysis of these structures under earthquake loading incorporating the product graph rules is presented for the first time. This formulation can generally be used for linear elastic dynamic analysis by accomplishing modal analysis. In the second part of this article, random vibration analysis of regular skeletal structures is performed via canonical forms and closed-form eigensolution of matrices containing repetitive patterns for symmetric structures. In this section, the formulation random dynamic analysis of the structures subjected to random seismic excitation as a random process in frequency domain is also presented. In the proposed methods, the main efficiency corresponds to the eigensolution of problems with significant computational effort reduction due to the efficient graph product rules and canonical form techniques being utilized for symmetric and cyclic symmetric structures. Numerical examples demonstrate the suitability and efficiency of the method for optimal structural dynamic analysis. Nevertheless, graph product based methods may also be applied to the random vibration analysis which is in a progressive state of development by the authors.

## References

- Brewer, J. (1978), "Kronecker products and matrix calculus in system theory", *IEEE Trans. Circuits Syst.*, **25**(9), 772-781.
- Chopra, A.K. (2012), *Dynamics of Structures*, 4<sup>th</sup> Edition, Pearson Education, Upper Saddle River.
- Clough, R.W. and Penzien, J. (2003), *Dynamics of Structures*, 3<sup>rd</sup> Edition, Computers and Structures, Berekely.
- El-Raheb, M. (2011), "Modal properties of a cyclic symmetric hexagon lattice", *Comput. Struct.*, **89**(23), 2249-2260.
- He, Y., Yang, H., Xu, M. and Deeks, A.J. (2013), "A scaled boundary finite element method for cyclically symmetric two-dimensional elastic analysis", *Comput. Struct.*, **120**, 1-8.
- Kangwai, R.D., Guest, S.D. and Pellegrino, S. (1999), "An introduction to the analysis of symmetric structures", *Comput. Struct.*, **71**(6), 671-688.
- Kaveh, A. (2013), *Optimal Analysis of Structures by Concepts of Symmetry and Regularity*, Springer, Wien-New York.
- Kaveh, A. and Nemati, F. (2010), "Eigensolution of rotationally repetitive space structures using a canonical form", *Int. J. Numer. Meth. Eng.*, **26**(12), 1781-1796.
- Kaveh, A. and Rahami, H. (2010), "An efficient analysis of repetitive structures generated by graph products", *Int. J. Numer. Meth. Eng.*, **84**(1), 108-126.
- Koohestani, K. and Kaveh, A. (2010), "Efficient buckling and free vibration analysis of cyclically repeated space truss structures", *Finite Elem. Anal. Des.*, **46**(10), 943-948.
- Koohestani, K. (2011), "An orthogonal self-stress matrix for efficient analysis of cyclically symmetric space truss structures via force method", *Int. J. Solid. Struct.*, **48**(2), 227-233.
- Kouachi, S. (2006), "Eigenvalues and eigenvectors of tridiagonal matrices", *Electron. J. Linear Algeb.*, **15**, 115-133.
- McDaniel, T.J. and Chang, K.J. (1980), "Dynamics of rotationally periodic large space structures", *J. Sound*

- Vib.*, **68**(3), 351-368.
- Newland, D.E. (2012), *An Introduction to Random Vibrations, Spectral and Wavelet Analysis*, 3<sup>rd</sup> Edition, Dover Publications, Mineola, New York.
- Olson, B.J., Shaw, S.W., Shi, C., Pierre, C. and Parker, R.G. (2014), "Circulant matrices and their application to vibration analysis", *Appl. Mech. Rev.*, **66**(4), 040803-1-040803-41.
- Rahami, H., Kaveh, A. and Shojaei, I. (2015), "Swift analysis for size and geometry optimization of structures", *Adv. Struct. Eng.*, **18**(3), 365-380.
- Shi, C. and Parker, R.G. (2014), "Vibration modes and natural frequency veering in three-dimensional, cyclically symmetric centrifugal pendulum vibration absorber systems", *J. Vib. Acoust.*, **136**(1), 011014.
- Shi, C. and Parker, R.G. (2015), "Vibration mode structure and simplified modelling of cyclically symmetric or rotationally periodic systems", *Proc. Roy. Soc. A*, doi: 10.1098/rspa.2014.0672.
- Thomas, D.L. (1979), "Dynamics of rotationally periodic structures", *Int. J. Numer. Meth. Eng.*, **14**(1), 81-102.
- Williams, F.W. (1986), "Exact eigenvalue calculations for structures with rotationally periodic substructures", *Int. J. Numer. Meth. Eng.*, **23**(4), 695-706.
- Yueh, W.-C. (2005), "Eigenvalues of several tridiagonal matrices", *Appl. Math. E-Notes*, **5**, 210-230.
- Zingoni, A. (2012), "Symmetry recognition in group-theoretic computational schemes for complex structural systems", *Comput. Struct.*, **94**, 34-44.
- Zingoni, A. (2014), "Group-theoretic insights on the vibration of symmetric structures in engineering", *Phil. Trans. R. Soc. A.*, **372**, 20120037.